International Journal of Solids and Structures 49 (2012) 1117–1126

Contents lists available at SciVerse ScienceDirect

International Journal of Solids and Structures

journal homepage: www.elsevier.com/locate/ijsolstr

An extended strain energy density failure criterion by differentiating volumetric and distortional deformation

Yujie Wei

State Key Laboratory of Nonlinear Mechanics, Institute of Mechanics, Chinese Academy of Sciences, Beijing 100190, PR China

ARTICLE INFO

Article history:
Received 25 July 2011
Received in revised form 12 January 2012
Available online 9 February 2012

Keywords:
Strain energy density
Fracture criterion
Crack kink
Pressure-dependent yielding
Distortional and volumetric

ABSTRACT

We extend Sih's strain energy density criterion (Sih, 1974) for crack kinks and material failure by weighting differently the volumetric and distortional parts in the extended strain energy density factor. The work is inspired by the factor that failure by microscopic shearing governed by distortion and microscopic separation controlled by hydrostatic tension represent distinct deformation processes, and should be treated differently as we count their influences to material failure. With the weight parameter introduced to the extended strain energy density factor criterion, we explain satisfactorily several critical experiments which reported crack kink in samples subjected to mixed-mode loading. The extended strain energy density idea is also used to derive a generalized pressure-dependent yielding criterion, which supplies a theoretical basis for those novel strength criteria for materials like bulk metallic glasses. Corresponding methods to determine the two material parameters, the critical strain energy density factor and the weight parameter quantifying the relative contribution by distortion over volumetric deformation, are discussed.

1. Introduction

When materials are initially cracked and are subjected to loads exceeding a certain level, the cracks will extend. Engineers are concerned about what methods could accurately predict crack propagation. With their endeavors in more than half century, now several physically rooted parameters are developed, among which including the energy release rate G (Griffith, 1921; Irwin, 1957), stress intensity factor K (Irwin, 1957), J-integral (Rice, 1968), crack-tip opening displacement δ_c (Wells, 1961; Cottrell, 1961), together with a recently developed criterion by taking an analogy of fracture with plasticity theory (Salvadori, 2008). There exist many applications by using aforementioned criteria. It is generally accepted that those criteria are better suited for materials with small scale yielding at the crack tip. For crack propagation in severely plastically deformed crack tips, those criteria face substantial challenges (e.g. Suo et al., 1992). In engineering practice, a crack is usually subjected to mixed-mode loading, and the crack could kink. It is of the interest of engineers to predict not only when the crack kinks but also the kink direction in both linear elastic and elastic–plastic materials.

In parallel to theoretical developments, numerical techniques like finite element method are broadly used to analyze crack propagation and crack kinks. One popular strategy is to insert cohesive zones (Barenblatt, 1959; Dugdale, 1960; Needleman, 1990; Xu and Needleman, 1994) along potential paths for crack extension, or by inserting virtual cohesive bonds between elements (Gao and Klein, 1998). Another promising methods is to use the extended-finite element method (Moes et al., 1999) which does not need to assume possible crack paths and minimizes the troublesome remeshing. In those numerical experiments, crack propagation and kinks could be governed by stress criterion, separation criterion, energy criterion, or a combination of them, and those local quantities could be directly connected to global criteria such as G and J_c.

Theoretically, while several methods could be applied to predict cracking paths (see the summary by Salvadori (2010)), there are two broadly used criteria to describe crack kinks: the maximum circumferential stress criterion suggested by Erdogan and Sih (1963) and the strain energy density (SED) factor criterion developed by Sih (1974). The maximum circumferential stress criterion postulates that

> *a crack under mixed-mode loading advances in a direction in which the greatest value of circumferential (hoop) stress reaches a critical magnitude;*

and the SED factor criterion predicts that

> *the location of fracture coincides with the site of relative minimum strain energy density factor.*

Successful applications of the maximum circumferential stress criterion are mainly for brittle materials. For mixed-mode crack problems and in materials with intermediate to large plastic

E-mail address: yujie_wei@lnm.imech.ac.cn

0020-7683/$ - see front matter © 2012 Elsevier Ltd. All rights reserved.
doi:10.1016/j.ijsolstr.2012.01.015

deformation, fracture may not be governed by only one of the six independent stress components (Gdoutos, 1990). In addition, the critical stress quantity can not be used to describe the fracture resistance, which is specimen geometry and size dependent. These shortages of the maximum circumferential stress criterion motivated the development of the SED factor criterion. A series of successful applications by using the SED factor criterion for both brittle and ductile materials could be seen in Sih (1974, 1991).

While the SED criterion works well in many applications, it does not always give satisfactory predictions. Experiments by Finnie and Weiss (1974) to investigate crack propagation in beryllium sheet showed inconsistence between experimental result and the prediction by using the SED factor criterion. The kink angle in a 45° inclined crack is about −50° by experiments but that from SED prediction is −34°. In addition, since SED criterion used one parameter – the critical strain energy density factor – to quantify failure, it predicts a constant mode II to mode I fracture toughness ratio for all materials with the same Poisson's ratio, e.g., $K_{IIc}/K_{Ic} = 0.9$ for $\nu = 0.33$, which might be physically questionable. Also, the ratio that $K_{IIc}/K_{Ic} = 0.9$ when $\nu = 0.33$ could be underestimated since it is commonly known that K_{IIc} is greater than K_{Ic} in many face-centered-cubic (f.c.c.) metals.

Another motivation to extend the SED criterion is to connect the fracture criterion with microscopic deformation mechanisms. The evolution of mode I fracture toughness K_c with sample thickness may examplify the distinction between failure governed by distortion and that by dilatation, see Fig. 1. In thin plate when microscopic shearing dominates (thickness $\leqslant B_m$) failure, the insufficient development of strain hardening limits the size of the plastic zone. As the sample thickness B increases, further hardening of materials gives rise to increasing of plastic zone and hence enhanced fracture toughness K_c. The fracture toughness reaches its maximum when the sample is so thick that the transition of failure from shearing mode to dilatation mode at the microscopic level occurs. Fracture toughness keeps dropping till crack extension is completely formed by separation, where $K_c = K_{Ic}$. In view of the difference between shear failure and separation failure at the microscopic level, we expect that the distortional part and the volumetric part of the SED should be weighted differently to assess material failure.

The focus of the paper is to extend the SED factor criterion by taking account the difference in microscopic deformation mechanisms for material failure. The program of this paper is as follows. We present the extended strain energy density criterion for material failure in Section 2. In Section 3, we show applications of the extended SED model to a central crack under several typical conditions including mode I, mode II, and mixed-mode loading. The predictability of the extended SED model is given in Section 4 for mixed-mode inclined cracks. In Section 5, we show that the extended SED model may be also applied to describe pressure-dependent material yielding. We close in Section 6 with some concluding remarks.

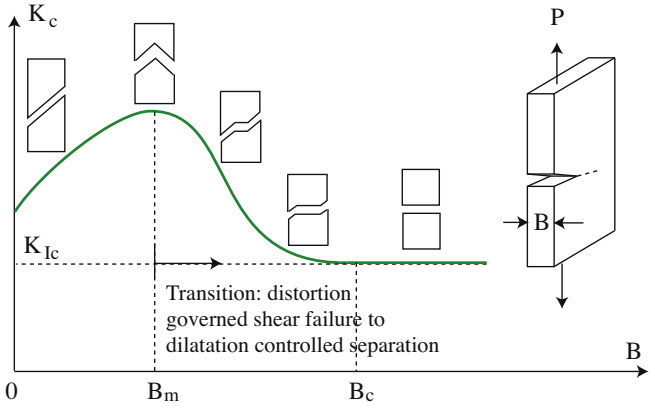

Fig. 1. Illustration of the fracture toughness variation with sample thickness B, which demonstrates the transition from distortion controlled shearing failure to dilation governed separation renders the drop of K_c to K_{Ic} as the sample thickness changes from B_m to B_c.

2. The extended strain energy density factor criterion

For a material subjected to general stress state ($\sigma_x, \sigma_y, \sigma_z, \tau_{xy}, \tau_{yz}, \tau_{zx}$) in a Cartesian coordinate (x,y,z), the total strain energy per unit volume dW/dV is given as

$$\frac{dW}{dV} = \frac{1+\nu}{2E}\left[\sigma_x^2+\sigma_y^2+\sigma_z^2-\frac{\nu}{1+\nu}(\sigma_x+\sigma_y+\sigma_z)^2+2\left(\tau_{xy}^2+\tau_{yz}^2+\tau_{zx}^2\right)\right] \tag{1}$$

where E and ν are the Young's modulus and Poisson's ratio of an isotropic material. It is easy to verify that dW/dV can be decomposed into a distortional part dW_d/dV with

$$\frac{dW_d}{dV} = \frac{1+\nu}{6E}\left[(\sigma_x-\sigma_y)^2+(\sigma_y-\sigma_z)^2+(\sigma_z-\sigma_x)^2+6\left(\tau_{xy}^2+\tau_{yz}^2+\tau_{zx}^2\right)\right] \tag{2}$$

and a volumetric part dW_v/dV with

$$\frac{dW_v}{dV} = \frac{1-2\nu}{6E}(\sigma_x+\sigma_y+\sigma_z)^2 \tag{3}$$

If we write the above equations in the principal stress coordinate axes ($\sigma_1, \sigma_2, \sigma_3$) and recall that the octahedral shear stress is given as

$$\tau_{oct} = \frac{1}{3}\left[(\sigma_1-\sigma_2)^2+(\sigma_2-\sigma_3)^2+(\sigma_3-\sigma_1)^2\right]^{1/2} \tag{4}$$

the distortional and volumetric strain energy density could now be simplified as

$$\frac{dW_d}{dV} = \frac{3(1+\nu)}{2E}\tau_{oct}^2 = \frac{3}{4\mu}\tau_{oct}^2 \tag{5}$$

and

$$\frac{dW_v}{dV} = \frac{3(1-2\nu)}{2E}p^2 = \frac{p^2}{2\kappa} \tag{6}$$

respectively. Here p is the hydrostatic tension (positive in tension and negative in compression) and is defined as $p \equiv (\sigma_1+\sigma_2+\sigma_3)/3$, and μ and κ are the shear modulus and the bulk modulus, respectively.

Sih (1974, 1991) postulated that a crack would extend in a direction where the strain energy density factor is minimized and reaches a critical value S_c. Now we differentiate the failure governed by distortional and volumetric strain energy density factors. For the special case of hydrostatic tension governed failure, we have

$$r_0\frac{dW_v}{dV} = r_0\frac{p^2}{2\kappa} \leqslant S_v \tag{7}$$

where S_v is the critical strain energy density associated with failure governed by normal stress and r_0 is the radius of a core region (see Fig. 2). It is noted that we count the contribution of Eq. (7) to failure only when $p > 0$. If the solid is subjected to pure distortion,

$$r_0\frac{dW_d}{dV} = r_0\frac{3}{4\mu}\tau_{oct}^2 \leqslant S_d \tag{8}$$

where S_d is the critical strain energy density factor associated with failure controlled by distortion. Combining Eqs. (7) and (8), we obtain a unified fracture criterion which couples the influences by distortion and hydrostatic tension

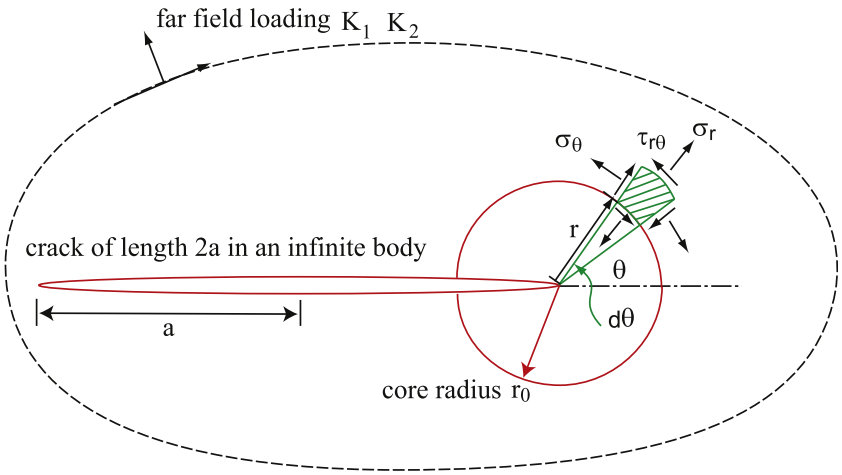

Fig. 2. Illustration of a crack under far-field mixed-mode loading k_1 and k_2. The stress components σ_r, σ_θ and $\tau_{r\theta}$ ahead of the crack tip expressed in the cylindrical polar coordinates (r,θ) in the core region with radius r_0 are also shown.

$$\frac{dW_d}{dV}\frac{r_0}{S_d}+\frac{dW_v}{dV}\frac{r_0}{S_v}\leqslant 1 \tag{9}$$

The above equation can be given in a more straightforward way as

$$\frac{3}{4\mu}\tau_{oct}^2+\frac{p^2}{2\kappa}\left(\frac{S_d}{S_v}\right)\leqslant\frac{S_d}{r_0} \tag{10}$$

For a crack under far-field mixed-mode loading k_1 and k_2 shown in Fig. 2, its stress components σ_r, σ_θ and $\tau_{r\theta}$ ahead of the crack tip are given by Williams (1957):

$$\sigma_r=\sqrt{\frac{2}{r}}[k_1(3-\cos\theta)\cos(\theta/2)+k_2(3\cos\theta-1)\sin(\theta/2)]+\cdots \tag{11a}$$

$$\sigma_\theta=\sqrt{\frac{2}{r}}[k_1(1+\cos\theta)\cos(\theta/2)-k_2(3\sin\theta)\cos(\theta/2)]+\cdots \tag{11b}$$

$$\tau_{r\theta}=\sqrt{\frac{2}{r}}[k_1\sin\theta\cos(\theta/2)+k_2(3\cos\theta-1)\cos(\theta/2)]+\cdots \tag{11c}$$

Now Eqs. (7) and (8) can be rewritten as

$$r_0\frac{dW_v}{dV}=b_{11}k_1^2+b_{12}k_1k_2+b_{22}k_2^2 \tag{12}$$

and

$$r_0\frac{dW_d}{dV}=c_{11}k_1^2+c_{12}k_1k_2+c_{22}k_2^2 \tag{13}$$

respectively. Sih (1991) had derived the coefficients b_{ij} and c_{ij} $(i,j=1,2,3)$, which are given as

$$b_{11}=(1-2\nu)(1+\nu)(1+\cos\theta)/12\mu \tag{14a}$$

$$b_{12}=-(1-2\nu)(1+\nu)(1+\sin\theta)/12\mu \tag{14b}$$

$$b_{22}=(1-2\nu)(1+\nu)(1-\cos\theta)/12\mu \tag{14c}$$

and

$$c_{11}=(1+\cos\theta)[1-\cos\theta+2(1-2\nu)^2/3]/16\mu \tag{15a}$$

$$c_{12}=2\sin\theta[\cos\theta-(1-2\nu)^2/3]/16\mu \tag{15b}$$

$$c_{22}=[4-3\sin^2\theta+2(1-2\nu)^2(1-\cos\theta)/3]/16\mu \tag{15c}$$

where μ is the shear modulus. Let $S_d/S_v=\beta$, we define an extended strain energy density factor $\bar{S}$ as

$$\begin{aligned}\bar{S}&=r_0\frac{dW_d}{dV}+\beta r_0\frac{dW_v}{dV}\\&=(\beta b_{11}+c_{11})k_1^2+(\beta b_{12}+c_{12})k_1k_2+(\beta b_{22}+c_{22})k_2^2\end{aligned} \tag{16}$$

When $\beta=1$, $\bar{S}$ would reduce to the SED factor expression given by Sih (1974). With Eq. (16), we extend the SED failure criterion by Sih (1974) and make the following hypotheses on crack initiation in a two-dimensional crack problem:

(1) The initial crack growth occurs in the direction (θ_0) along which the strain energy density factor $\bar{S}$ is minimized, i.e.

$$\partial\bar{S}/\partial\theta=0|_{\theta=\theta_0}=0,\ \text{and}\ \partial^2\bar{S}/\partial\theta^2|_{\theta=\theta_0}\geqslant 0 \tag{17}$$

where θ_0 satisfies $-\pi<\theta_0<\pi$.

(2) Crack extends if the strain energy density factor $\bar{S}$ defined in Eq. (16) reaches the critical value $\bar{S}_c$ at $\theta=\theta_0$.

We shall explore the features of the extended SED criterion under the influence of β and show its predictability to available crack kink experiments in the next sections.

3. Application of the extended SED model

3.1. Central crack in tension

We consider the special case of a central crack in tension with crack plane normal to the loading axis, i.e., $\phi=\pi/2$ in Fig. 3a. In this case, $k_1=\sigma\sqrt{a}$ and $k_2=0$, and the extended SED is written as

$$\begin{aligned}\bar{S}=\frac{(1+\cos\theta)k_1^2}{48\mu}&[4\beta(1-2\nu)(1+\nu)+2(1-2\nu)^2\\&+3(1-\cos\theta)]\end{aligned} \tag{18}$$

The direction of crack extension is determined by solving

$$\sin\theta_0[3\cos\theta_0-2\beta(1-2\nu)(1+\nu)-(1-2\nu)^2]=0 \tag{19}$$

for θ_0. It is convenient to obtain the two solutions, which are given as

$$\theta_0=0$$

or

$$\theta_0=\operatorname{acos}\left[\frac{2\beta(1-2\nu)(1+\nu)+(1-2\nu)^2}{3}\right] \tag{20}$$

By applying the second condition in Eq. (17), we get the solution which predicts that the crack extends along $\theta_0=0$, and is independent on β. The second solution corresponds to the direction of the

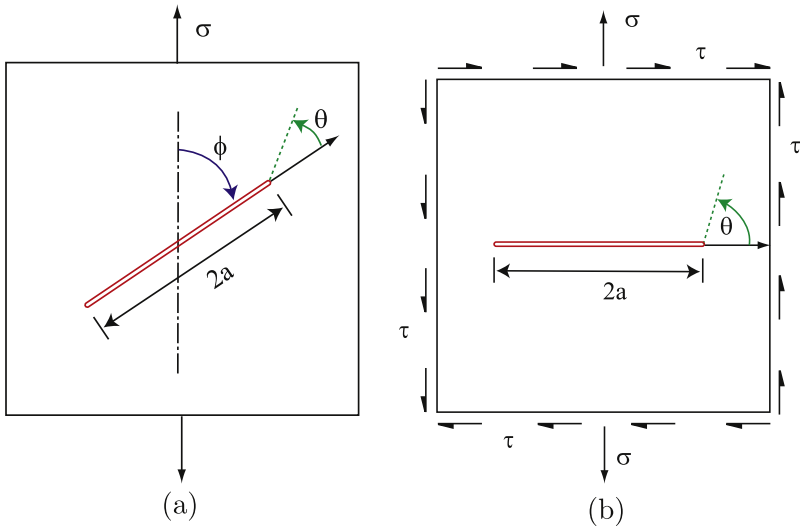

Fig. 3. Illustration of cracks subjected to different loading modes: (a) an inclined crack under tension, and (b) a central flat crack under mixed-mode loading.

maximum strain energy density. We hypothesize that there exist both minimum and maximum SEDs, which requires β to satisfy

$$0 < \beta < \frac{3-(1-2\nu)^2}{2(1-2\nu)(1+\nu)} \tag{21}$$

Eq. (21) also implies that the right-hand side would be greater than zero, which leads to $\nu > (1-\sqrt{3})/2 \approx -0.366$. When $\beta \to 0$, the crack under mode I loading will extend in the crack plane. As β approaches the upper bound, the SED factor maximizes at $\theta = 0$. Its minimum occurs in the direction perpendicular to the crack if we take a physically meaningful solution for θ. The limits for β also set the lower bound for the Poisson's ratio: the validity of Eq. (21) requires the Poisson's ratio to be in the range of $(-0.366, 0.5)$. Fig. 4 shows the dependence of the maximum β on Poisson's ratio. For what follows, we shall discuss fracture behavior when β satisfies Eq. (21).

3.2. Central crack in shearing

When the crack is subjected to far field pure shearing, as shown in Fig. 3b (with $\sigma = 0$), we have $k_1 = 0$ and $k_2 = \tau\sqrt{a}$. The extended SED factor is given as

$$\bar{S} = \frac{k_2^2}{48\mu}\{2(1-2\nu)(1-\cos\theta)[(1-2\nu)+2\beta(1+\nu)] + 3 + 9 \times \cos^2\theta\} \tag{22}$$

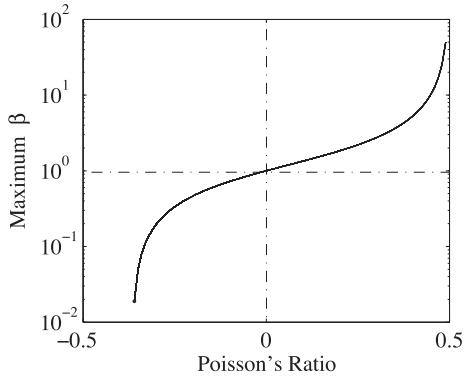

Fig. 4. The dependence of the maximum β on Poisson's ratio.

The direction of crack extension satisfies $\partial\bar{S}/\partial\theta|_{\theta=\theta_0} = 0$, and is determined by solving

$$\sin\theta_0[2\beta(1-2\nu)(1+\nu)+(1-2\nu)^2 - 9\cos\theta_0] = 0 \tag{23}$$

for θ_0. The two solutions to Eq. (23) for θ_0 are obtained as

$$\theta_0 = 0$$

and

$$\theta_0 = \operatorname{acos}\left[\frac{2\beta(1-2\nu)(1+\nu)+(1-2\nu)^2}{9}\right] \tag{24}$$

It is convenient to see that the crack under pure shear will extend along the direction given in Eq. (24). The solution $\theta_0 = 0$ is excluded by applying the minimum $\bar{S}$ condition. We also notice from this expression there exists a requirement for β

$$0 < \beta \leqslant \frac{9-(1-2\nu)^2}{2(1-2\nu)(1+\nu)} \tag{25}$$

which is satisfied since our discussion for β is confined by Eq. (21). The fracture angle for the central crack under shear versus β for several Poisson's ratios are plotted in Fig. 5. For small β, which cor-

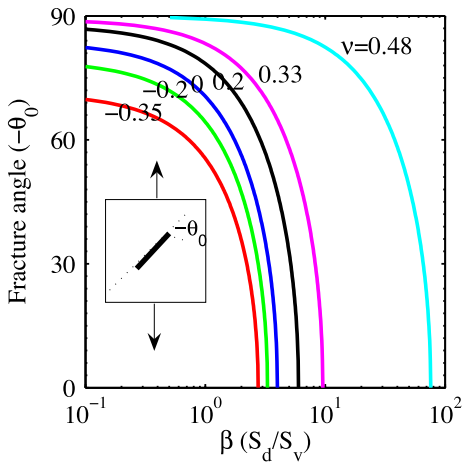

Fig. 5. The fracture angle versus β for fracture in a central crack under pure shear. Corresponding curves for several Poisson's ratios show the influence by Poisson's ratio as well.

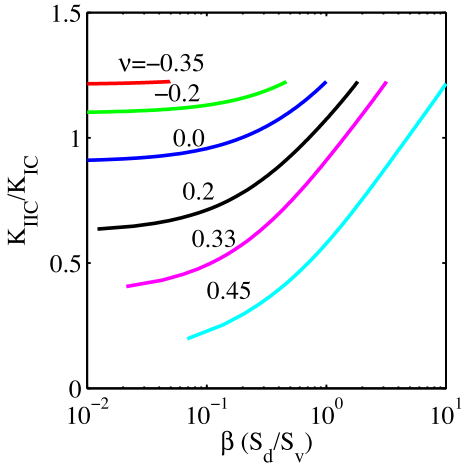

Fig. 6. Dependence of K_{IIC}/K_{IC} on β for materials with different Poisson's ratio.

responds to the case of larger critical volumetric SED factor S_v in contrast to the critical distortional SED factor S_d, the crack will kink from the original crack plane dramatically; as β reaches its maximum at a given Poisson's ratio, the crack shall propagate along the original crack plane.

3.3. Central crack in mixed-mode loading

In this subsection, we explore fracture behavior in cracks under mixed-mode loading, i.e., a combination of shearing and tensile loading applied to the crack shown in Fig. 3b. The far field loading are given as $k_1 = \sigma\sqrt{a}$ and $k_2 = \tau\sqrt{a}$. By using Eq. (16), we could obtain $\bar{S}_c$ for the case of $k_2 = 0$, which can be expressed in terms of K_{Ic},

$$\bar{S}_c = \frac{(1-2\nu)[2\beta(1+\nu)+(1-2\nu)]K_{Ic}^2}{12\mu}, \quad \text{for } K_{Ic} = \sigma_c\sqrt{a} \tag{26}$$

Similarly, by setting $k_1 = 0$ and $k_2 = K_{IIc}$ such that $\bar{S} = \bar{S}_c$, we could establish the relationship between K_{Ic} and K_{IIc}, which is found to follow

$$\left(\frac{K_{IIc}}{K_{Ic}}\right)^2 = \frac{4(1-2\nu)[2\beta+1+2(\beta-1)\nu]}{2(1-2\nu)(1-\cos\theta_0)[(1-2\nu)+2\beta(1+\nu)]+3+9\cos^2\theta_0} \tag{27}$$

where θ_0 is given by Eq. (24). The dependence of K_{IIC}/K_{IC} upon β for materials with different Poisson's ratio is demonstrated in Fig. 6. It is seen that K_{IIC}/K_{IC} increases as β increases. For each Poisson's ratio, K_{IIC}/K_{IC} reaches its maximum of $\sqrt{6}/2 = 1.22$ as β reaches its maximum given in Eq. (21). For the case of mixed-mode fracture, we could construct the $k_1 - k_2$ locus for fracture of the central crack by setting $\bar{S} = \bar{S}_c$ in Eq. (16), where θ_0 is determined for each combination of k_1 and k_2 by applying the conditions given in Eq. (17). Corresponding fracture envelope for the crack in Fig. 2 are given in Fig. 7. Here the cases for $\nu = -0.2, 0, 0.33$, and *0.45* are shown in Fig. 7a to d, respectively. Both Poisson's ratio and β have significant impact to the mixed-mode fracture envelope, and the influence becomes stronger as ν increases. The non-convex fracture envelope in Fig. 7d for $\beta = 0.2$ could be due to high critical volumetric SED and low compressibility (a Poisson's ratio of 0.45) in the material.

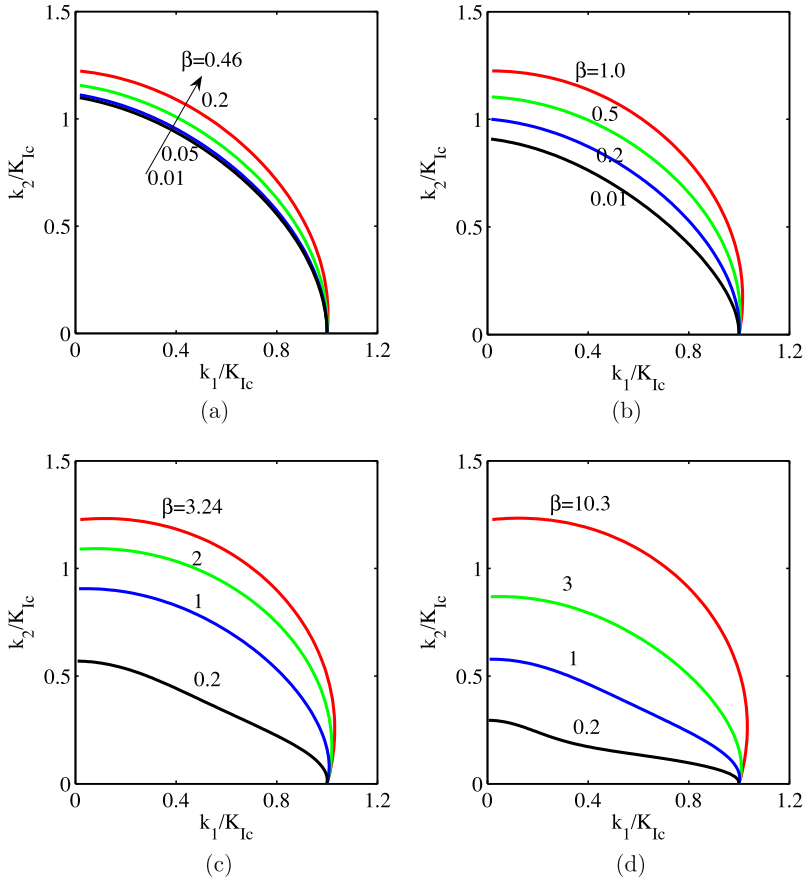

Fig. 7. Mixed-mode fracture envelope for cracks under loading shown in Fig. 1 under the influence of Poisson's ratio. (a) $\nu = -0.2$, (b) $\nu = 0$, (c) $\nu = 0.333$, and (d) $\nu = 0.45$.

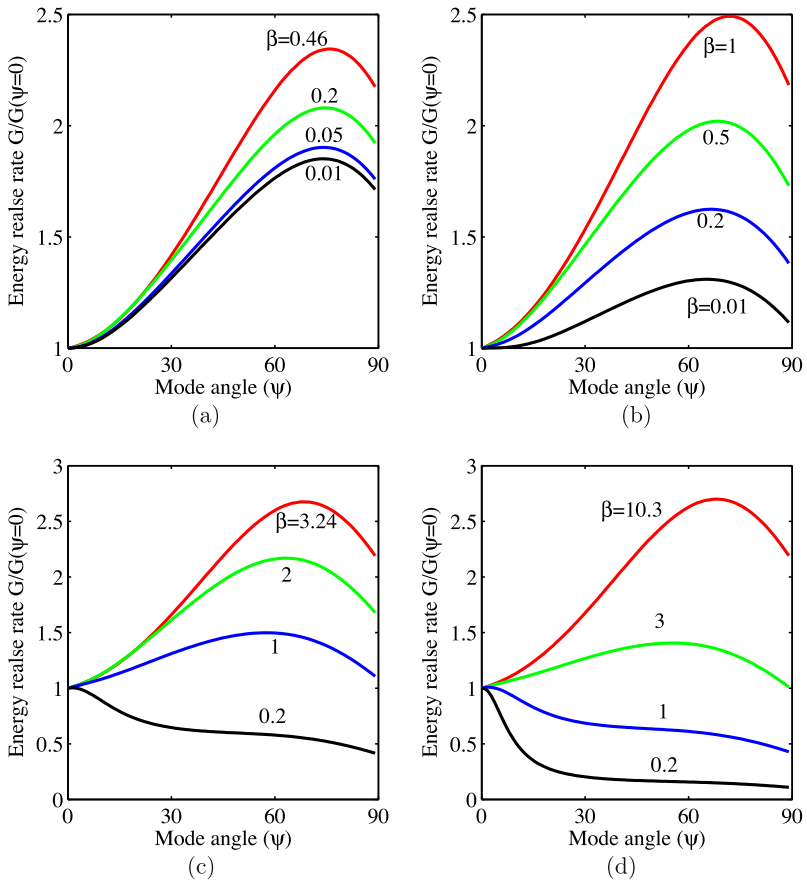

Fig. 8. Strain energy release rate versus mode angle for different Poisson's ratio and β. (a) $v = -0.2$, (b) $v = 0$, (c) $v = 0.33$, and (d) $v = 0.45$. Here G is normalized by the energy release rate at $\psi = 0$.

Correspondingly, we could also calculate the strain energy release rate G for the plane strain cracking problem (Irwin, 1957)

$$G = \frac{(1-v^2)\left(K_I^2 + K_{II}^2\right)}{E} \tag{28}$$

For kinked cracks, the stress intensity factors K_I and K_{II} at the kink tip could be calculated from the applied stress intensity factors to the primary crack (Williams, 1957; Bilby and Cardew, 1975; Lawn and Wilshaw, 1975; Bilby et al., 1977; Cotterell and Rice, 1980; Ichikawa and Tanaka, 1982; Suresh and Shih, 1986; Leblond, 1989; Amestoy and Leblond, 1992; Leblond and Frelat, 2000; Suo et al., 2010). Here we adopt the formulae given by Amestoy and Leblond (1992) for stationary crack with infinitesimal branching. In their derivation, K_I and K_{II} are related to k_1 and k_2 as

$$K_I = a_{11}k_1 + a_{12}k_2 \tag{29a}$$

$$K_{II} = a_{21}k_1 + a_{22}k_2 \tag{29b}$$

where

$$a_{11} = 1 - \frac{3\pi^2}{8}m^2 + \left(\pi^2 - \frac{5\pi^4}{128}\right)m^4 + \left(\frac{\pi^2}{9} - \frac{11\pi^4}{72} + \frac{119\pi^6}{15360}\right)m^6 + 5.07790m^8 - 2.88312m^{10} - 0.0925m^{12} + 2.996m^{14} - 4.059m^{16} + 1.63m^{18} + 4.1m^{20} + O(m^{22}); \tag{30a}$$

$$a_{12} = -\frac{3\pi}{2}m + \left(\frac{10\pi}{3} + \frac{\pi^3}{16}\right)m^3 + \left(-2\pi - \frac{133\pi^3}{180} + \frac{59\pi^5}{1280}\right)m^5 + 12.313906m^7 - 7.32433m^9 + 1.5793m^{11} + 4.0216m^{13} - 6.915m^{15} + 4.21m^{17} + 4.56m^{19} + O(m^{21}); \tag{30b}$$

$$a_{21} = \frac{\pi}{2}m - \left(\frac{4\pi}{3} + \frac{\pi^3}{48}\right)m^3 + \left(-\frac{2\pi}{3} + \frac{13\pi^3}{30} - \frac{59\pi^5}{3840}\right)m^5 - 6.176023m^7 + 4.44112m^9 - 1.5340m^{11} - 2.0700m^{13} + 4.684m^{15} - 3.95m^{17} - 1.32m^{19} + O(m^{21}); \tag{30c}$$

$$a_{22} = 1 - \left(\frac{4+3\pi^2}{8}m^2\right) + \left(\frac{8}{3} + \frac{29\pi^2}{18} - \frac{5\pi^4}{128}\right)m^4 + \left(-\frac{32}{15} - \frac{4\pi^2}{9} - \frac{1159\pi^4}{7200} + \frac{119\pi^6}{15360}\right)m^6 + 10.58254m^8 - 4.78511m^{10} - 1.8804m^{12} + 7.280m^{14} - 7.591m^{16} + 0.25m^{18} + 12.5m^{20} + O(m^{22}). \tag{30d}$$

Here $m = \theta_0/\pi$. Note that k_1 and k_2 in Eq. (29b) satisfies $\overline{S} = \overline{S}_c$ in Eq. (16). Fig. 8a–d shows respectively strain energy release rate versus mode angle ψ ($\psi = \text{atan}(k_2/k_1)$) for Poisson's ratio $v = -0.2$ (Fig. 8a), $v = 0$ (Fig. 8b), $v = 0.33$ (Fig. 8c), and $v = 0.45$ (Fig. 8d). While the impact of β to G is small for $v = -0.2$, its effect becomes significant for $v > 0$. When $v = 0.33$ and $v = 0.45$, the normal trend that G increases monotonically as ψ increases could completely changed as β varies.

4. Predictability of the SED model for kinks in inclined cracks

Since most available experiments on mixed-mode loading were performed for inclined cracks, we show in this section the predictability of the extended SED model on crack kinking. For the inclined crack seen in Fig. 3a, we have $k_1 = \sigma\sqrt{a}\sin^2\phi$ and $k_2 = \sigma\sqrt{a}\sin\phi\cos\phi$. With Eq. (16) and using the condition that $\partial\overline{S}/\partial\theta = 0$, we have

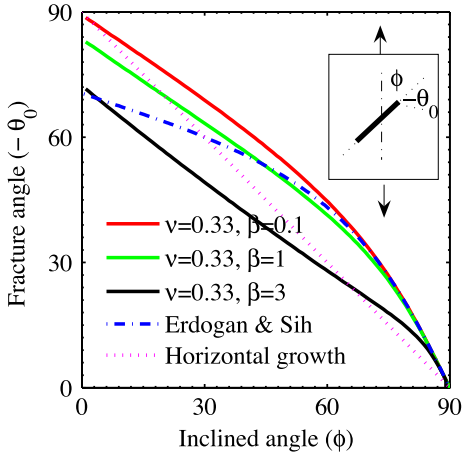

Fig. 9. The fracture angle versus inclined angle during the propagation of an inclined crack under tension. Theoretical predictions from different models are shown, and the influence of β at $\nu = 0.33$ predicted by this work is also demonstrated.

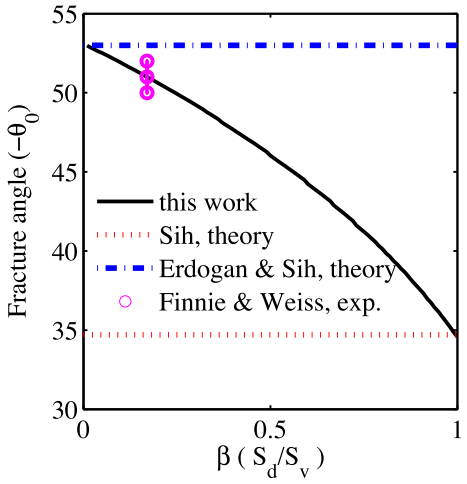

Fig. 10. The fracture angle in inclined crack under tension for beryllium sheets. Experimental data (Finnie and Weiss, 1974) and theoretical prediction from different models are presented. Here the Poisson's ratio $\nu = 0$ is used, and the influence of β to fracture angle is significant.

$$\frac{\partial \bar{S}}{\partial \theta}\frac{48\mu}{\sigma^2 a} = \sin^2\phi\{2(1-2\nu)[1+2\beta+2(\beta-1)\nu]\sin(\theta-2\phi) - 3\sin(2\theta) - 6\sin(2\theta-2\phi)\} \quad (31)$$

For $\phi \neq 0$, the crack kink direction is determined by solving the following equation

$$2(1-2\nu)[1+2\beta+2(\beta-1)\nu]\sin(\theta_0-2\phi) - 3\sin(2\theta_0) - 6\sin(2\theta_0-2\phi) = 0 \quad (32)$$

for θ_0. Corresponding solutions for several β at $\nu = 0.33$ are shown in Fig. 9.

As a comparison, the fracture angles at different inclined angles predicted by different theories are shown in Fig. 9. The kink angle θ_0 predicted by the maximum circumferential stress criterion (Erdogan and Sih, 1963) is determined by solving

$$\sin\theta_0 + (3\cos\theta_0 - 1)\cot\phi = 0 \quad (33)$$

for θ_0 at a given ϕ. In their experiments for beryllium sheet, Finnie and Weiss (1974) observed that the initially inclined crack with $\phi = 45°$ branched with $\theta_0 \approx -50°$. The SED theory by Sih (1974) predicts $\theta_0 \approx -34°$. Fig. 10 shows the predicted kink angles by different theories and experimental data. The extended SED theory predicts that the kink angle is a function of β, and fits well to experimental results if $\beta \approx 0.2$. It means that the critical strain energy for separation failure is greater than that for distortional failure, which seems to be reasonable for the hexagonal-close-packed beryllium polycrystals where its basal slip resistance is very low in contrast to its separation strength. Note that in this special case, the results from our work with $\beta \to 0$ matches the prediction based on the maximum circumferential stress criterion by Erdogan and Sih (1963), and that with $\beta \to 1$ equals to what predicted by Sih's (1974) SED criterion.

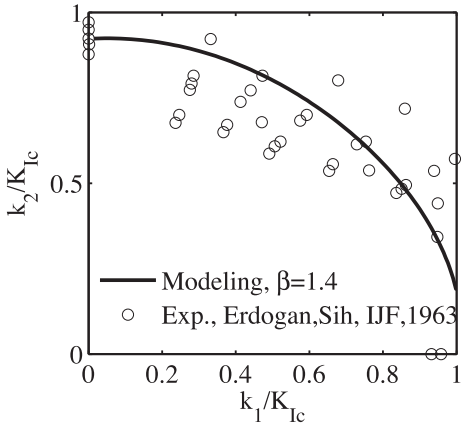

Fig. 11. The fracture envelope from experiments and modeling. Experimental data come from Erdogan and Sih (1963) for PMMA. We have used a Poisson' ratio $\nu = 0.37$ and $\beta = 1.4$ for the model.

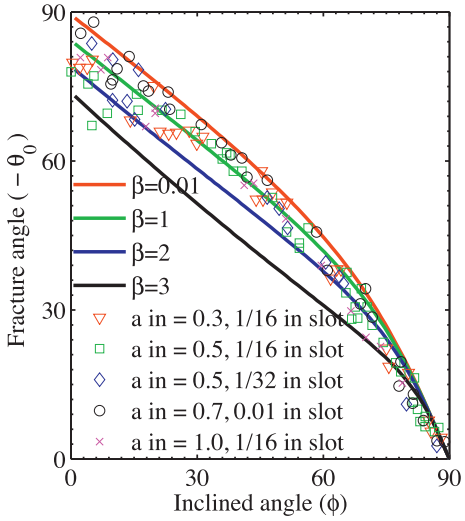

Fig. 12. The fracture angle in initially inclined crack under tension under the influence of β for plexiglass, theoretical prediction versus experimental results are shown.

The fracture envelope for polymethylmethacrylate (PMMA) from both experiments and theoretical prediction is shown in Fig. 11. Here we use a Poisson's ratio $\nu = 0.37$ for PMMA and $\beta = 1.4$ in the model. A reasonable agreement between experimental data and theoretical prediction is observed. Curves of fracture angle versus inclined angle for pre-cracked PMMA sheets are shown in Fig. 12. Theoretical predictions using $\beta \leqslant 1.0$ match well with experimental results reported by Williams and Ewing (1984).

From Fig. 3a, we also expect that kinks will occur in the inclined crack if uniaxial compression is applied, and the fracture angle cor-

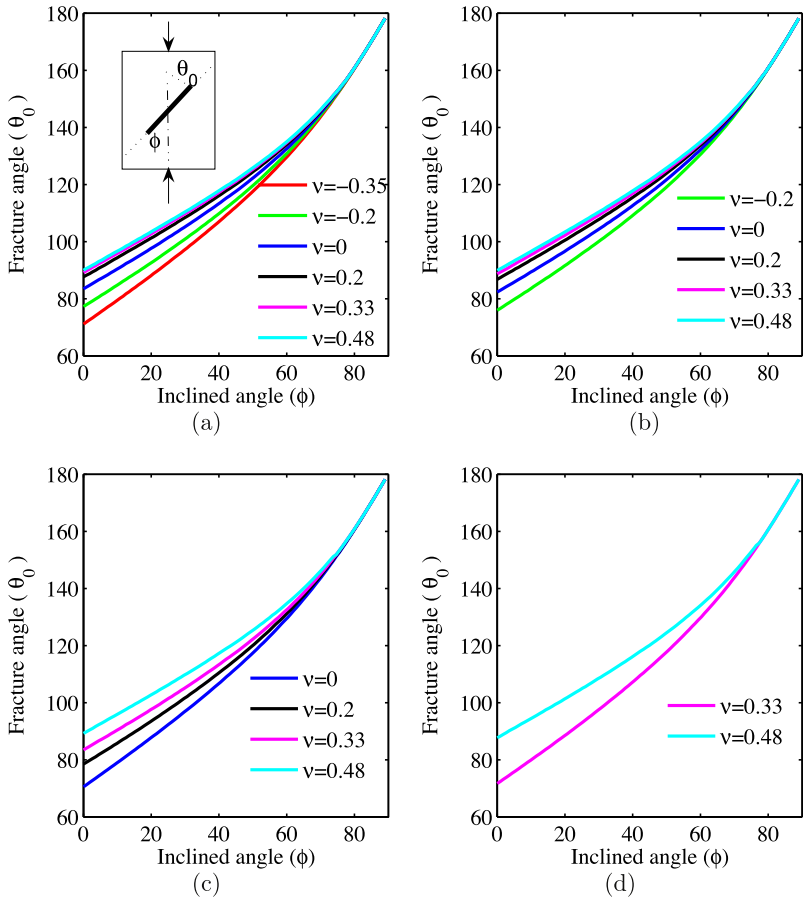

Fig. 13. Fracture angle versus inclined angles ϕ for several β. (a) $\beta = 0.01$, (b) $\beta = 0.1$, (c) $\beta = 1$, and (d) $\beta = 5$.

responds to the solution of positive θ_0 to Eq. (32). The plots of fracture angle against inclined angle ϕ for the inclined crack subjected to compression are given in Fig. 13, with Fig. 13a to d correspond to $\beta = 0.01, 0.1, 1$, and 5, respectively. In Fig. 14, corresponding fracture angles versus β are shown for several initial inclined angle ϕ, and Fig. 14a–d correspond to $\phi = 0°, 35°, 45°$, and 75°, respectively.

5. Pressure-dependent yielding criterion using extended SED

We discuss in this section the possibility of utilizing the extended SED idea for material yielding. In fact, we show that the von-Mises criterion (von Mises, 1913) is a special case of the extended yielding criterion since it only uses the distortional part of the SED, i.e.

$$\frac{dW_d}{dV} = \frac{3\tau_{oct}^2}{4\mu} \leqslant \frac{3}{4\mu}\left(\sqrt{\frac{2}{3}}\tau_y\right)^2 \tag{34}$$

Here the relationship $\tau_{oct} = \sqrt{2/3}\tau_y$ is derived on the basis of yielding at pure shear. To account for pressure dependent yielding, we define an cavitation (separation) strength p_c such that

$$\frac{dW_v}{dV} = \frac{p^2}{2\kappa} \leqslant \frac{1}{2\kappa}p_c^2 \tag{35}$$

The final yielding envelope, by assuming the additive contributions from distortional and volumetric SED to macroscopic yielding, is given in the form of

$$\frac{3}{2}\left(\frac{\tau_{oct}}{\tau_y}\right)^2 + \left(\frac{p}{p_c}\right)^2 \mathrm{sgn}(p) \leqslant 1 \tag{36}$$

If we take an analogy of the above yielding envelope to a cohesive model, τ_{oct} corresponds to the shearing component applied upon the interface with normal along [111] direction in the principal stress coordination, and p is the normal traction on the plane. So Eq. (36) supplies a coupled interfacial yielding criterion, with $\sqrt{2/3}\,\tau_y$ being the macroscopic shearing strength and p_c being the maximum resistance to interfacial separation. Note that physically, τ_y and p_c are two independent concepts. An intuitive explanation on this is that the presence of dislocations in an atomic plane would dramatically change the resistance to relative gliding between the top and the bottom blocks separated by the plane, i.e., τ_y drops, but has minor impact to p_c.

We further note that the yielding envelope defined by Eq. (36) shows a pressure-dependent shearing strength,

$$\tau_{oct} \leqslant \sqrt{\frac{2}{3}}\tau_y\sqrt{1 - \mathrm{sgn}(p)\left(\frac{p}{p_c}\right)^2} \tag{37}$$

which resembles the broadly used Mohr–Coulomb law for pressure-dependent shearing. Taking a simple tensile test as a model case, we see that the pressure dependence of the above yielding criterion gives

$$\sigma_t = \frac{3\tau_y}{\sqrt{3 + \left(\frac{\tau_y}{p_c}\right)^2}} \tag{38}$$

where σ_t is the tensile yield strength. The corresponding yield strength in compression σ_c is obtained to be

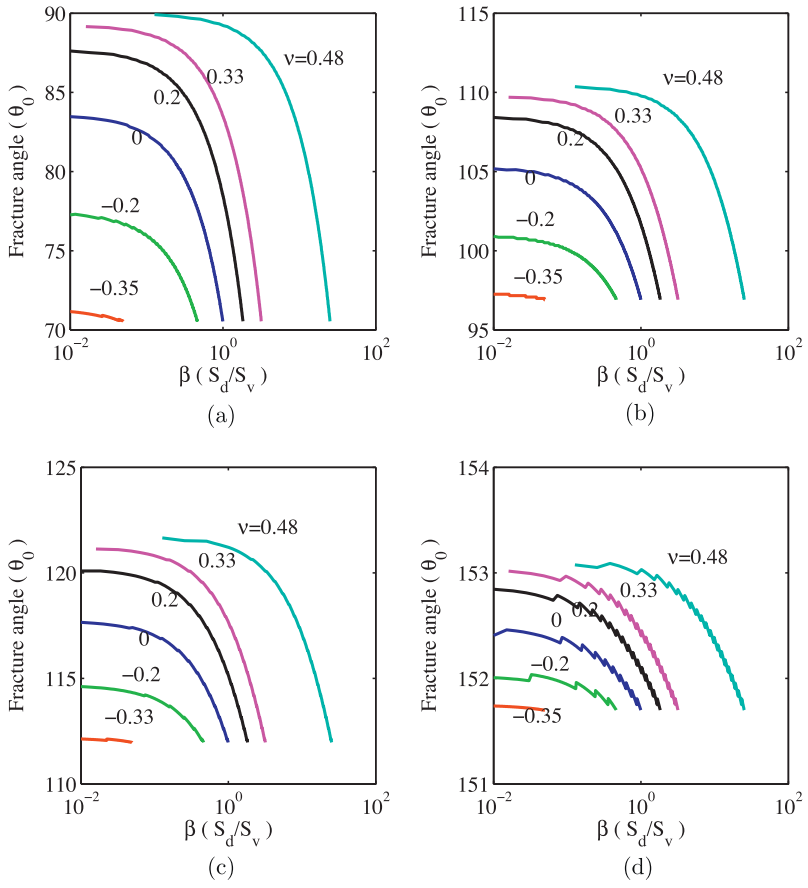

Fig. 14. Fracture angle versus β in inclined cracks with different ϕ under uniaxial compression. (a) $\phi = 0$, (b) $\phi = 30°$, (c) $\phi = 45°$, and (d) $\phi = 75°$.

$$\sigma_c = \frac{3\tau_y}{\sqrt{3 - \left(\frac{\tau_y}{p_c}\right)^2}} \tag{39}$$

The yielding asymmetry is governed by the material's shearing strength and separation strength:

$$\Delta\sigma = \sigma_c - \sigma_t = \sqrt{3}\tau_y\left(\frac{\tau_y}{p_c}\right)^2, \quad \text{for } \tau_y/p_c \ll 1 \tag{40}$$

We note that p_c cannot be derived from uniaxial tensile or compressive yielding strength. For the relationships $\sigma_y = 3.06\tau_c$ and $\tau_y = \sqrt{3}\tau_c$ which connects the dislocation slip resistance τ_c in f.c.c. single crystals with the tensile strength σ_y and shearing strength τ_y in their polycrystalline counterparts, they rely on the factor that the same type of microslips by dislocations (Taylor, 1938; Bishop and Hill, 1952) accounts for plastic deformation. However, p_c measures the separation strength of atomic layers, and it approximates to the ideal strength and is about $E/3 \sim E/10$ for crystalline metals. Commonly, τ_y or σ_y is at least one to two magnitude smaller than that. Therefore, Eq. (36) explains why polycrystalline metals usually show negligible pressure-dependence in yielding. In most granular materials (see Paterson, 1958; Lockner, 1995) or amorphous metals (e.g. Schuh and Lund, 2003; Anand and Su, 2005; Zhang and Eckert, 2005; Chen et al., 2011) where p_c could be comparable to τ_y due to the initial presence of flaws or excessive free volume, they show perceivable pressure-sensitive yielding. If p_c is small and the volumetric part in Eq. (36) is significant, the volumetric SED governs material failure and the material is expected to be brittle; alternatively, the material could be ductile if the distortional part is dominant. Those qualitative predictions by Eq. (36) are consistent with previous brittle-to-ductile transition criteria developed by Kelly et al. (1967) and by Rice and Thomson (1974).

6. Discussion and concluding remarks

To conclude, we introduce here an extended SED factor criterion for material failure, which differentiates the weight of volumetric and distortional contributions to the extended SED factor. Such an extension reflects the physical difference of microscopic shearing and microscopic separation in materials undergoing fracture. It further amends the weakness of the original SED factor criterion which predicts a constant model II to mode I fracture toughness ratio for all materials with the same Poisson's ratio regardless their microstructural discrepancies. Applications of the model to available experiments show its good predictability to kink problems in inclined cracks. While the critical extended SED factor can be readily obtained from their mode I fracture toughnesses for most materials, an additional experiment, either pure mode II or mixed-mode loading test, is needed to determine the weight parameter β. For example, if we have the mode II fracture toughness at hand, β could be determined by using Eq. (27) if the Poisson's ratio of the material is also known; in case we had corresponding information for kink angle from a crack subjected to mixed-mode loading, β could then be found by utilizing Eq. (32). With both β and $\bar{S}c$, material failure could be determined by applying the theory for regular geometries and by computational techniques for arbitrary geometries. While the extended SED model takes the microscopic distortion and separation into account during fracture, we note that the model at this stage is incapable of bridge micro- to atomic-scale deformation

mechanisms in crack tips (e.g.Rice, 1992; Tadmor and Hai, 2003) to a macroscopic description.

At the end, we also postulate a material yielding criterion based on the extended SED idea by accounting for the microscopic shearing and microscopic separation mechanisms differently. The generalized yielding criterion reduces to the von Mises yielding criterion (von Mises, 1913) if the material has high cavitation (separation) strength. It also resembles the Mohr–Coulomb law for pressure-dependent shearing, as seen in most granular materials and amorphous metals. The yielding criterion based on SED supplies a theoretical basis for recently proposed pressure-dependent strength criterion for metallic glasses (e.g. Schuh and Lund, 2003; Anand and Su, 2005; Zhang and Eckert, 2005; Chen et al., 2011). From Eq. (37), we see the "internal friction" which gives rise to pressure-dependent yielding is related to the shear strength and the cavitation (separation) strength of a material, which might be respectively obtained from simple shearing tests and plane strain tension tests.

Acknowledgements

Supports from CAS Hundred Talent Project, KJCX2-EW-L03, 973 Project (2011CB711103), and NSFC grant (11021262) are acknowledged.

References

Amestoy, M., Leblond, J.B., 1992. Crack paths in plane situations II. Detailed form of the expansion of the stress intensity factors. Int. J. Solids Struct. 29, 465–501.
Anand, L., Su, C., 2005. A theory for amorphous viscoplastic materials undergoing finite deformations, with application to metallic glasses. J. Mech. Phys. Solids 53, 1362–1396.
Barenblatt, G.I., 1959. The formation of equilibrium cracks during brittle fracture: general ideas and hypotheses, axially symmetric cracks. Appl. Math. Mech. (PMM) 23, 622–636.
Bishop, J., Hill, R., 1952. A theory of the plastic distortion of a polycrystalline aggregate under combined stresses. Phil. Mag. 42, 1298–1307.
Bilby, B.A., Cardew, G.E., 1975. The crack with a kinked tip. Int. J. Fracture 11, 708–712.
Bilby, B.A., Cardew, G.E., Howard, I.C., 1977. Stress intensity factors at the tip of kinked and forked cracks. In: Taplin, D.M.R. (Ed.), Fracture, vol. 3. University of Waterloo Press, pp. 197–200.
Chen, Y., Jiang, M.Q., Wei, Y.J., Dai, L.H., 2011. Failure criterion for metallic glasses. Phil. Mag. 91, 4536–4554.
Cottrell, A.H., 1961. Theoretical aspects of radiation damage and brittle fracture in steel pressure vessels. In: Steels for reactor pressure circuits, Iron and Steel Institute, Special Report No. 69, p. 281.
Cotterell, B., Rice, J.R., 1980. Slightly curved or kinked cracks. Int. J. Fracture 16, 155–169.
Dugdale, D.S., 1960. Yielding of steel sheets containing slits. J. Mech. Phys. Solids 8, 100–104.
Erdogan, E., Sih, G.C., 1963. On the crack extension in plates under plane loading and transverse shear. J. Basic Eng. 85D, 519–525.
Finnie, I., Weiss, H.D., 1974. Some observations on Sih's strain energy density approach for fracture prediction. Int. J. Fracture 10, 136–138.
Gao, H., Klein, P., 1998. Numerical simulation of crack growth in an isotropic solid with randomized internal cohesive bonds. J. Mech. Phys. Solids 46, 187–218.
Gdoutos, E.E., 1990. Fracture Mechanics Criteria and Applications. Kluwer Academic Publishers.
Griffith, A.A., 1921. The phenomena of rupture and flow in solids. Phil. Trans. Roy. Soc. Lond., A 221, 163–198.
Ichikawa, M., Tanaka, S., 1982. A critical analysis of the relationship between the energy release rate and the SIFs for non-coplanar crack extension under combined mode loading. Int. J. Fracture 18, 19–28.
Irwin, G., 1957. Analysis of stresses and strains near the end of a crack traversing a plate. J. Appl. Mech. 24, 361–364.
Kelly, A., Tyson, W.R., Cottrell, A.H., 1967. Ductile and brittle crystals. Phil. Mag. 15, 567–586.
Lawn, B., Wilshaw, T.R., 1975. Fracture of Brittle Solids. Cambridge University Press.
Leblond, J.B., 1989. Crack paths in plane situations I. General form of the expansion of the stress intensity factors. Int. J. Solids Struct. 25, 1311–1325.
Leblond, J.B., Frelat, J., 2000. Crack kinking from an initially closed crack. Int. J. Solids Struct. 37, 1595–1614.
Lockner, D.A., 1995. Rock failure. In: Ahrens, T.J. (Ed.), Rock Physics and Phase Relations: A Handbook of Physical Constants. The American Geophysical Union, pp. 127–147.
Moes, N., Dolbow, J., Belytschko, T., 1999. A finite element method for crack growth without remeshing. Int. J. Numer. Methods Eng. 46, 131–150.
Needleman, A., 1990. An analysis of decohesion along an imperfect interface. Int. J. Fracture 40, 21–40.
Paterson, M.S., 1958. Experimental deformation and faulting in Wombeyan marble. Bull. Geol. Soc. Am. 69, 465–476.
Rice, J.R., 1968. A path independent integral and the approximate analysis of strain concentration by notches and cracks. J. Appl. Mech. 35, 379–386.
Rice, J.R., 1992. Dislocation nucleation from a crack tip: an analysis based on the Peierls concept. J. Mech. Phys. Solids 40, 239–271.
Rice, J.R., Thomson, R., 1974. Ductile versus brittle behaviour of crydstals. Phil. Mag. 29, 73–97.
Salvadori, A., 2008. A plasticity framework for (linear elastic) fracture mechanics. J. Mech. Phys. Solids 56, 2092–2116.
Salvadori, A., 2010. Crack kinking in brittle materials. J. Mech. Phys. Solids 58, 1835–1846.
Schuh, C.A., Lund, A.C., 2003. Atomistic basis for the plastic yield criterion of metallic glass. Nature Mater. 2, 449–452.
Sih, G.C., 1974. Strain-energy-density factor applied to mixed mode crack problems. Int. J. Fracture 10, 305–321.
Sih, G.C., 1991. Mechanics of Fracture Initiation and Propagation. Kluwer, Boston.
Suo, Z.G., et al., 2010. Mixed-Mode Fracture. Curved Crack Path. <http://imechanica.org/node/8036>.
Suo, Z., Kuo, C.M., Barnett, D.M., Willis, J.R., 1992. Fracture mechanics for piezoelectric ceramics. J. Mech. Phys. Solids 40, 739–765.
Suresh, S., Shih, C.F., 1986. Plastic near-tip fields for branched cracks. Int. J. Fracture 30, 237–259.
Tadmor, E.B., Hai, S., 2003. A Pererls criterion for the onset of deformation twnning at crack tips. J. Mech. Phys. Solids 51, 765–793.
Taylor, G.I., 1938. Plastic strain in metals. J. Inst. Metals 62, 307–324.
von Mises, R., 1913. Mechanik der festen Körper im plastisch deformablen zustand. Göttin. Nachr. Math. Phys. 1, 582–592.
Wells, A.A., 1961. Unstable crack propagation in metals: cleavage and fast fracture. Proceeding of the Crack Propagation Symposium, vol. 1. College of Aeronautics and Royal Aeronautics Society, Cranfield, England, pp. 201–230.
Williams, M.L., 1957. On the stress distribution at the base of a stationary crack. J. Appl. Mech. 24, 109–114.
Williams, J.G., Ewing, P.D., 1984. Fracture under complex stress – the angled crack problem. Int. J. Fracture 26, 346–351.
Xu, X.P., Needleman, A., 1994. Numerical simulations of fast crack growth in brittle solids. J. Mech. Phys. Solids 42, 1397–1434.
Zhang, Z.F., Eckert, J., 2005. Unified tensile fracture criterion. Phys. Rev. Lett. 94, 094301.